Moment-method calculations of scattering by a square plate using singular basis functions and multipole expansions

Andersson, Tommy

Published in:
Journal Electromagnetic Waves and Applications

1993

Link to publication

Citation for published version (APA):
Andersson, T. (1993). Moment-method calculations of scattering by a square plate using singular basis functions and multipole expansions. *Journal Electromagnetic Waves and Applications*, *7*(1), 93-121.

Total number of authors:
1

LUND UNIVERSITY

PO Box 117
221 00 Lund
+46 46-222 00 00

CODEN:LUTEDX/(TEAT-7014)/1-28/(1991)

Moment-method calculations of scattering by a square plate using singular basis functions and multipole expansions

Tommy Andersson

Department of Electroscience
Electromagnetic Theory
Lund Institute of Technology
Sweden

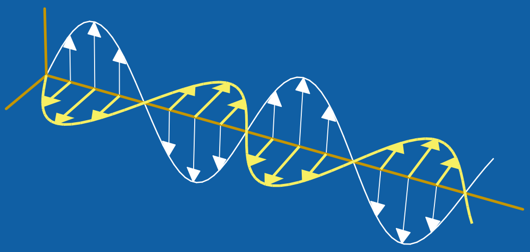

Tommy Andersson

Department of Electromagnetic Theory
Lund Institute of Technology
P.O. Box 118
SE-221 00 Lund
Sweden

Editor: Gerhard Kristensson

Abstract

The method of moments is used to solve electromagnetic boundary value problems numerically. It is known that the choice of basis functions is crucial for the numerical efficiency. Fast convergence is achieved provided the basis functions efficiently approximate the unknown function. In this paper the far field (incl. RCS) of a thin conducting square plate is calculated. Basis functions with correct edge and corner singularities are shown to greatly enhance the convergence compared to ordinary "rooftop" functions. The calculations of the matrix elements as well as the right side of the matrix equation and the scattered field are simplified by the use of a multipole technique.

1 Introduction

The method of moments (MoM) [1] has been used extensively during the last two decades to solve electromagnetic boundary value problems. By a projection technique a linear operator equation is replaced by a finite dimensional matrix equation suited for numerical treatment. MoM involves the expansion of an unknown function in terms of a set of basis functions. The choice of these basis functions is of great importance for the efficiency of the numerical computations.

It is desirable that the set of basis functions meet the following three properties:

1. They should allow simple and fast computations of the matrix elements.
2. They should be adaptable to different shapes of the domain.
3. They should efficiently approximate the unknown function, thus reducing the truncation size of the matrix.

Entire domain (global) basis functions have been shown to give excellent approximations when known properties of the function to determine are taken into account [2]-[4]. However, it seems difficult, especially in the three dimensional case, to adapt these basis functions for more general problems.

Subdomain basis functions of simple structure, e.g., so-called "rooftop" functions are often used to expand the current density [5], [6]. These functions are adapted to different shapes of the domain and easy to handle numerically, but in cases when the unknown function has a singular behaviour, e.g., at edges and corners of a thin scatterer, the subsections have to be very small to get high accuracy.

In the two-dimensional case, the use of rooftop functions in the interior of the domain in conjunction with singular basis functions at the edges, clearly improves the accuracy [7], [8]. Basis functions with correct edge behaviour have also been used in some three-dimensional cases [9], [10]. Recently, a three-dimensional static case where the corner singularity was incorporated in the basis functions was treated by the author [11]. The use of basis functions with both correct edge and corner singularities was shown to greatly enhance the convergence. To facilitate the numerical treatment a multipole method was adopted. The free space Green function for the Helmholtz equation was expanded in terms of the spherical scalar wave functions. Using subdomain basis and testing functions, the non-diagonal matrix elements could be expressed as a series of multipole moments [11].

In this paper, the multipole approach is applied to a canonical dynamic case - scattering by a perfectly conducting, infinitely thin, square plate. Basis functions with singularities corresponding to the known behaviour of the source distributions at the edges and corners are used. The multipole method is shown to be an efficient tool, not only for calculating the matrix elements, but also for calculating the right side of the matrix equation. Moreover, the scattered field and the radar cross section can be expressed and efficiently handled numerically by the means of the multipole method.

The plan of the paper is as follows. In Section 2 the scattering equation is derived and the testing procedure is defined. In Section 3 the basis and testing functions are described. The calculation of the matrix elements is treated in Section 4. This section contains an overview of the multipole technique and its implementation in this dynamic case together with a method to calculate the self-patch terms. In Sections 5 and 6 the multipole concept is applied to calculate the right side of the matrix equation and to calculate the scattered field. Numerical results are presented in Section 7 illustrating the enhanced convergence due to the singular basis functions and also showing the radar cross section for various frequencies and angles of incidence. Some conclusions are given in Section 8. Appendix A contains some mathematical details, while definitions and formulas concerning the scalar spherical wave functions are presented in Appendix B.

2 Scattering equation and testing procedure

In this section an integral equation for the surface current induced by an incident electromagnetic wave on a thin conducting scatterer is formulated. By expanding the current in a set of basis functions and applying a testing procedure this equation is replaced by a matrix equation suited for numerical treatment. The formulation is well-known, cf., e.g., Refs. [5] and [6], but for the sake of completeness and to introduce our notation an outline of the derivation is given for a flat thin conducting scatterer.

Let S denote a surface in the x-y-plane, which coincides with the thin perfectly conducting scatterer, cf. Fig. 1. The permeability and permittivity of surrounding media are μ and ε, respectively. $\boldsymbol{E}^{in}$ denotes the electric field of the incident wave in the absence of the scatterer. The induced surface current density $\boldsymbol{J}$ generates a scattered field $\boldsymbol{E}^{sc}$. $\boldsymbol{J}$ represents the vector sum of the surface current densities on the opposite sides of the scatterer. A harmonic time dependence is assumed and the time factor $e^{-i\omega t}$ is suppressed everywhere.

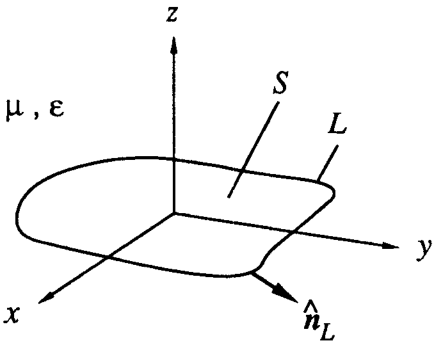

Fig. 1. The thin conducting scatterer and the Cartesian coordinates.

The integral equation

The scattered electric field $\boldsymbol{E}^{sc}$ due to the induced current density $\boldsymbol{J}$ can be expressed as

$$\boldsymbol{E}^{sc} = -\nabla V + i\omega \boldsymbol{A} \qquad (1)$$

where the scalar potential V and the magnetic vector potential $\boldsymbol{A}$ are given by

$$V(\boldsymbol{r}) = \frac{1}{\varepsilon} \int_S \sigma(\boldsymbol{r}')\, G(\boldsymbol{r},\boldsymbol{r}')\, \mathrm{d}S' \tag{2}$$

and

$$\boldsymbol{A}(\boldsymbol{r}) = \mu \int_S \boldsymbol{J}(\boldsymbol{r}')\, G(\boldsymbol{r},\boldsymbol{r}')\, \mathrm{d}S' \tag{3}$$

respectively.

The surface charge density σ is related to surface divergence of $\boldsymbol{J}$ through the equation of continuity,

$$\sigma = \frac{\nabla_S \cdot \boldsymbol{J}}{i\omega} \tag{4}$$

The surface divergence $\nabla_S \cdot \boldsymbol{J}$ is here $\partial_x J_x + \partial_y J_y$ since S is a surface in the x-y-plane. The free space Green function $G(\boldsymbol{r},\boldsymbol{r}')$ is defined as

$$G(\boldsymbol{r},\boldsymbol{r}') = \frac{\mathrm{e}^{ik|\boldsymbol{r}-\boldsymbol{r}'|}}{4\pi|\boldsymbol{r}-\boldsymbol{r}'|} \tag{5}$$

where the wave number $k = \omega\sqrt{\mu\varepsilon} = 2\pi/\lambda$.

The total electric field $\boldsymbol{E}$ is obtained as the vector sum of the incident field and the scattered field

$$\boldsymbol{E} = \boldsymbol{E}^{in} + \boldsymbol{E}^{sc} \tag{6}$$

Enforcing the boundary condition $\hat{z} \times \boldsymbol{E} = 0$ on S, one obtains the integral equation

$$\hat{z} \times (\nabla V - i\omega \boldsymbol{A}) = \hat{z} \times \boldsymbol{E}^{in}, \quad \boldsymbol{r} \text{ on } S \tag{7}$$

where V and $\boldsymbol{A}$ are given by Eqs. (2) and (3).

Notice that the limits on the left-hand side of Eq. (7) are well-defined quantities, since $\boldsymbol{A}(\boldsymbol{r})$ and the tangential derivatives $\hat{z} \times \nabla V$ are continuous on the surface S. The mathematical details of these limits can be found in, e.g., [12].

The matrix equation

The MoM is now applied to Eq. (7). This method is a projection method in which the integral equation is approximated by a matrix equation. This approximation is outlined below.

Expand the surface current density $\boldsymbol{J}$ in terms of a set of vector basis functions $\boldsymbol{f}_p$ with unknown coefficients a_p, i.e.,

$$\boldsymbol{J} = \sum_p a_p \boldsymbol{f}_p \tag{8}$$

It is assumed that the basis functions f_p are tangential to S, i.e., they have no $\hat{z}$-component. To satisfy the equation of continuity, Eq. (4), the expansion of the surface charge density σ will then become

$$\sigma = \frac{1}{i\omega}\sum_p a_p \ \nabla_S \cdot f_p \tag{9}$$

In the numerical treatment all summations have to be truncated.

The next step is to define a testing procedure. Let w_q be a set of testing functions and define a symmetric product as

$$<f,g> = \int_S f \cdot g \ \mathrm{d}S \tag{10}$$

Testing of Eq. (7) yields

$$<\nabla V, w_q> - i\omega <A, w_q> = <E^{in}, w_q> \tag{11}$$

The testing functions w_q are also assumed to be tangential to S. In addition to this requirement on w_q we chose testing functions such that

$$w_q \cdot \hat{n}_L = 0 \ \text{ on } L \tag{12}$$

where L is the boundary of S and $\hat{n}_L$ is the unit normal to L, cf. Fig. 1. Using the vector identity

$$\nabla_S \cdot (V \ w_q) = \nabla_S V \cdot w_q + V \ \nabla_S \cdot w_q \tag{13}$$

and Gauss' theorem in two dimension

$$\int_S \nabla_S \cdot (V \ w_q) \ \mathrm{d}S = \int_L V \ w_q \cdot \hat{n}_L \, \mathrm{d}l \tag{14}$$

one gets

$$<\nabla_S V, w_q> = -\int_S V \ \nabla_S \cdot w_q \ \mathrm{d}S \tag{15}$$

As $<\nabla_S V, w_q> = <\nabla V, w_q>$ on S, the matrix equation may now be explicitly expressed as

$$\sum_p a_p \int_S \int_S (-\nabla_S \cdot f_p(r') \ \nabla_S \cdot w_q(r) + k^2 f_p(r') \cdot w_q(r) \ ) \ G(r,r') \ \mathrm{d}S' \mathrm{d}S =$$

$$= i\omega\varepsilon \int_S E^{in}(r) \cdot w_q(r) \ \mathrm{d}S \qquad q = 1,2,3 \ldots \tag{16}$$

where $k^2 = \omega^2 \varepsilon u$.

3 Basis and testing functions

In the introduction of this paper the importance of the choice of the basis functions is pointed out. One conventional choice is subdomain basis functions, i.e., basis functions that only differ from zero over subsections of the domain. Due to the simplicity, we have chosen rectangular subsections. This limits the adaptation compared to subsections of triangular shape [6], [9]. However, the implementation of the main ideas to triangular subsections is possible, but has to be made to the price of a higher complexity in the analysis and the numerical treatment.

An overlapping technique is used to assure continuity of the current density in the direction of flow and thus preventing fictitious line charges at the connections of the basis functions. The scatterer is divided into equally sized "sub-squares". A basis function consists of two or three "sub-functions", each having support in one sub-square. The number of sub-squares necessary to achieve a certain accuracy of the solution depends on the ability of the basis functions to approximate the unknown function. As in our case, the behaviour of the unknown function, $\boldsymbol{J}$, differs over the domain we use different basis functions in the interior, at the edges and at the corners of the plate.

Interior basis functions

In the interior of the plate we use rooftop functions to approximate the surface current density $\boldsymbol{J}$. A rooftop function consists of two linear sub-functions, cf. Fig. 2. The resulting basis functions for the charge density will have the form of pulse doublets.

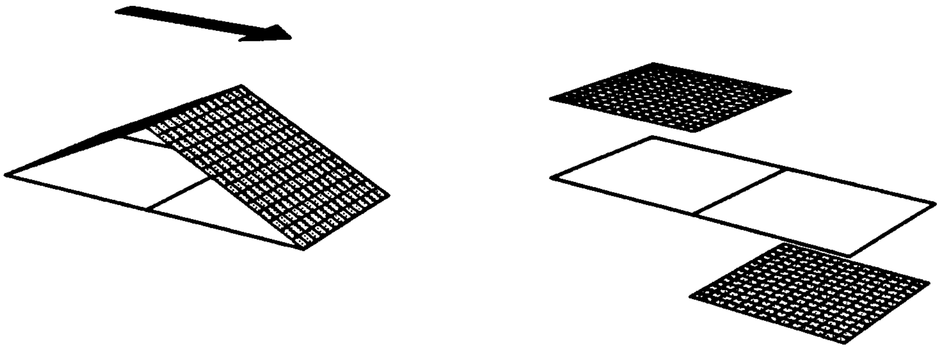
(a)

(b)

Fig. 2. The interior basis functions. The current is approximated by rooftop functions (a) and the charge by pulse doublets (b).

Edge basis functions

The singular behaviour of the surface current density and the surface charge density at the edge of an infinitely thin conducting scatterer has been investigated analytically [13] and is well-known. As the behaviour depends of the direction of the current in relation to the edge, two kinds of basis functions are needed.

Tangential current

To approximate the current tangential to an edge we use basis functions with the singularity $1/\sqrt{d}$, where d represents the perpendicular distance to the edge, but have a rooftop character in the direction along the edge, i.e., in the direction of flow. The principle form of the basis functions for the current density and the corresponding basis functions for the charge density are illustrated in Fig. 3.

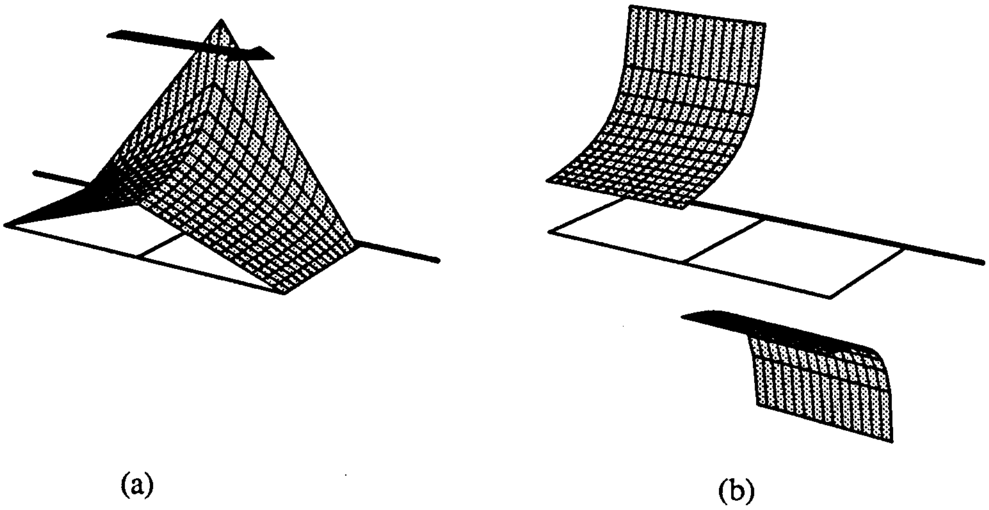

Fig. 3. The basis functions used to approximate the current tangential to an edge (a) and the corresponding charge distribution (b). Both functions have the singularity $1/\sqrt{d}$ near the edge.

Perpendicular current

The first order approximation of the behaviour of the current flowing perpendicular to the edge is $\sqrt{d}$, which agrees with $1/\sqrt{d}$ for the charge. We use basis functions with these singularities and which are constant in the direction along the edge. The continuity of the current density in the direction of flow at the connections to the interior sections, is guarantied by adding a half rooftop function, cf. Fig. 4.

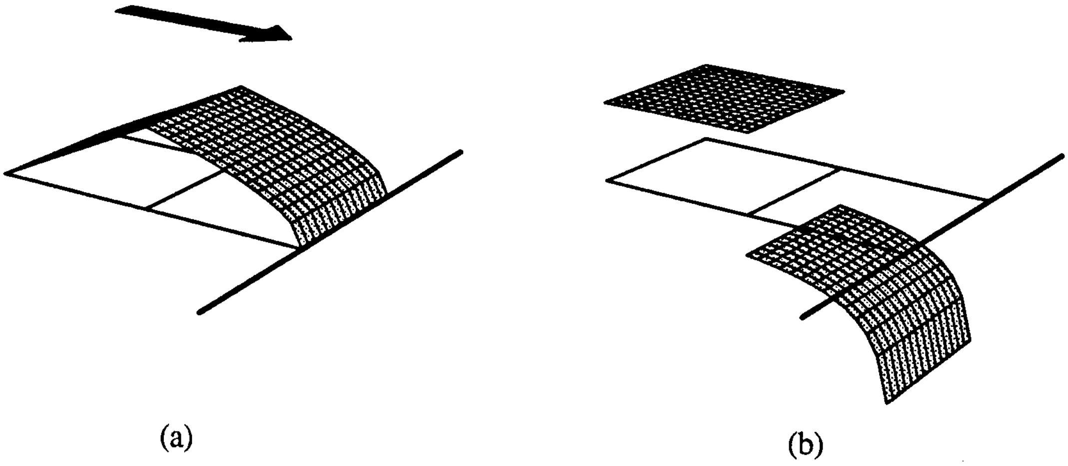

Fig. 4. The basis functions used to approximate the current perpendicular to an edge (a) and the corresponding charge distribution (b). The current basis function goes to zero as $\sqrt{d}$ near the edge resulting in the singularity $1/\sqrt{d}$ for the charge.

Corner basis functions

The field singularities at the tip of a conducting cone and as a limiting case, at the corner of a plane conducting sector, have been studied by some authors, i.e., [14], [15]. An exhaustive review of the subject can be found in [16]. The analysis shows that both the electric and the magnetic fields have singular properties. We use two sets of basis functions corresponding to these two different singularities. The first set is used to expand the current density flowing in the radial direction and the related accumulated charge density. These basis functions are constructed to give the correct singularity of the electric field. The second set is used to expand the current density flowing in the tangential direction and is constructed to give the correct singularity of the magnetic field.

Radial current

Introduce a local polar coordinate system with origin at the corner, cf. Fig. 5. Denote the sub-function for the radial current on the corner sub-square by f^{Cr}.

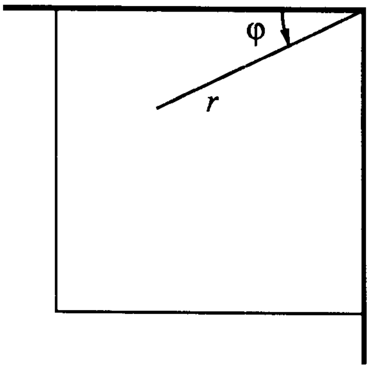

Fig. 5. The polar coordinate system used at corner sub-squares.

Define

$$f^{Cr} = \frac{r^{\nu}}{\sqrt{\sin\varphi\cos\varphi}}\hat{r} \tag{17}$$

and the corresponding basis sub-function for the charge density becomes

$$\nabla\cdot f^{Cr} = \frac{(\nu+1)\, r^{\nu-1}}{\sqrt{\sin\varphi\cos\varphi}} \tag{18}$$

These functions have the correct singular behaviour both at the edges and at the corner. The corner singularity of the charge density is given by the exponent $\nu-1$ with $\nu = 0.30$ according to [15]. The complete radial current basis functions are constructed by adding half rooftop functions with correct edge singularity at the adjacent edge sub-sections, cf. Fig. 6. The numerical treatment is simplified if the edge current basis sub-functions described above are used. This choice introduces a small discontinuity in the current density along the two lines connecting the sub-squares. The basis functions are normalized such that the total current across these lines is continuous. With this normalization the discontinuity along the lines is less than 8%. This type of discontinuity could, however, be remedied but to the price of a higher complexity in the analysis.

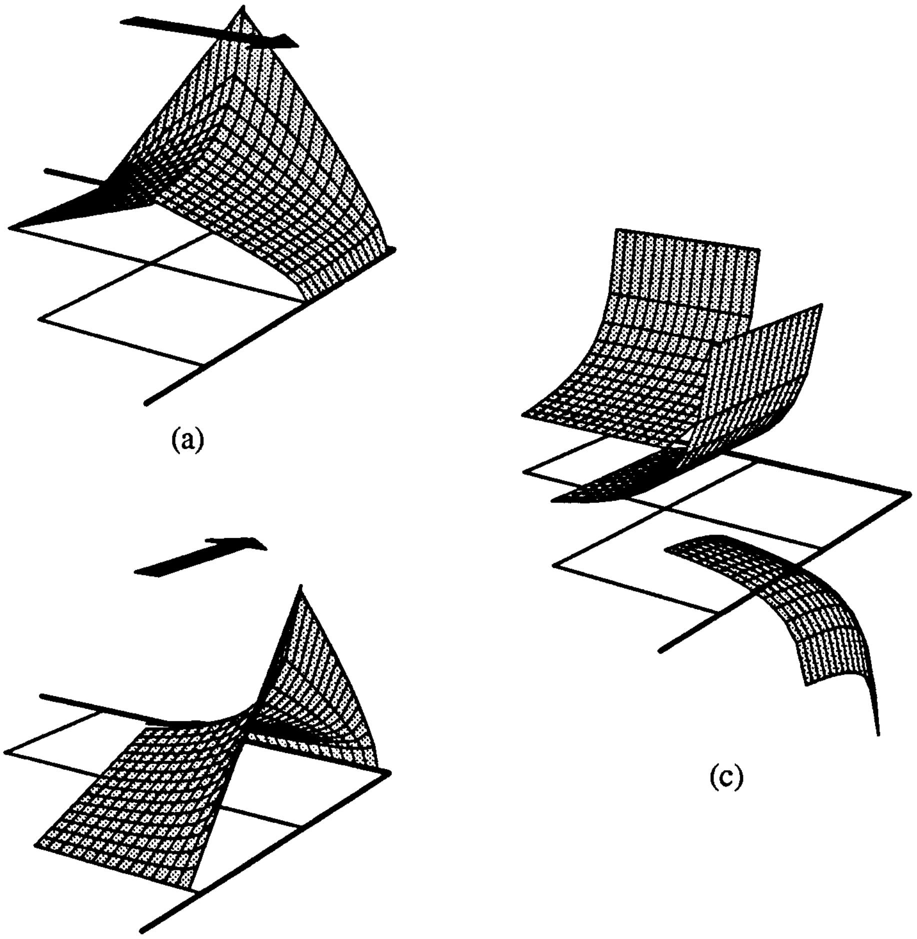

(a)

(b)

(c)

Fig. 6. The corner basis functions used to obtain the correct electric singularity. The Cartesian components of the basis function for the radial current are illustrated by (a) and (b). The corresponding basis function for the charge distribution is shown in (c).

Tangential current

Using the same polar coordinates as above introduce a potential Φ as

$$\Phi = r^{\tau}\sqrt{\sin\varphi\cos\varphi} \tag{19}$$

Define a sub-function f^{Ct} for the tangential current on the corner sub-square as

$$f^{Ct} = \hat{z} \times \nabla\Phi \tag{20}$$

where $\hat{z}$ denotes the unit normal to the surface S. This definition implies that $\nabla \cdot f^{Ct} = 0$ and the curves Φ = constant are lines of current. The equipotential lines are shown in Fig. 7. The lines do well agree with the corresponding lines of current presented in Ref. [15]. By the explicit expression of f^{Ct},

$$f^{Ct} = r^{\tau-1} \frac{\sin^2\varphi - \cos^2\varphi}{2\sqrt{\sin\varphi\cos\varphi}}\hat{r} + \tau r^{\tau-1}\sqrt{\sin\varphi\cos\varphi}\,\hat{\varphi} \tag{21}$$

it is evident that the correct edge behaviour is obtained. The numerical value of the singularity exponent is given by [15] as $\tau = 0.82$. The complete tangential current basis function is constructed in the same way as in the radial case described above by adding singular sub-functions at the adjacent edge sub-squares, cf. Fig. 8. The discontinuity of the current density along the two lines connecting the sub-squares will in this case be maximum 18 %.

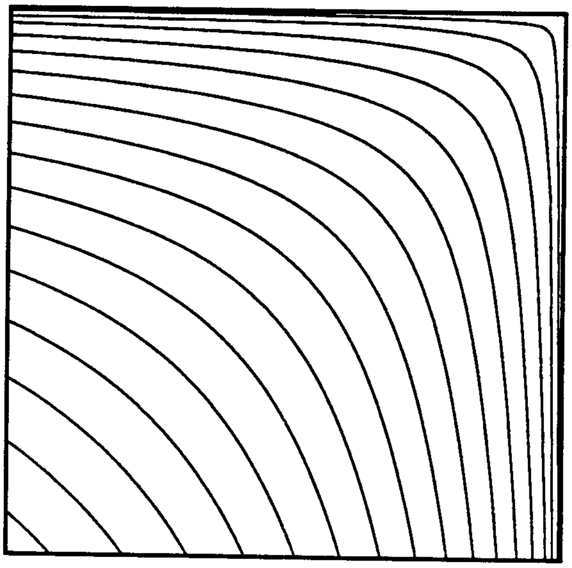

Fig. 7. Equipotential lines, i.e., lines of current. The difference of Φ between the lines is constant which implies that they enclose the same amount of current, cf. Appendix A.

Testing functions

The testing functions have to fulfil the requirements specified by Eq. (12), i.e., the normal component has be zero at the edges of the scatterer. As all the basis functions described above have this property they can be used as testing functions. In the numerical treatment we have made two choices: 1.Testing functions equal to the basis functions, i.e., Galerkin's method. 2.Testing functions equal to rooftop functions. The results are presented and discussed in Section 7.

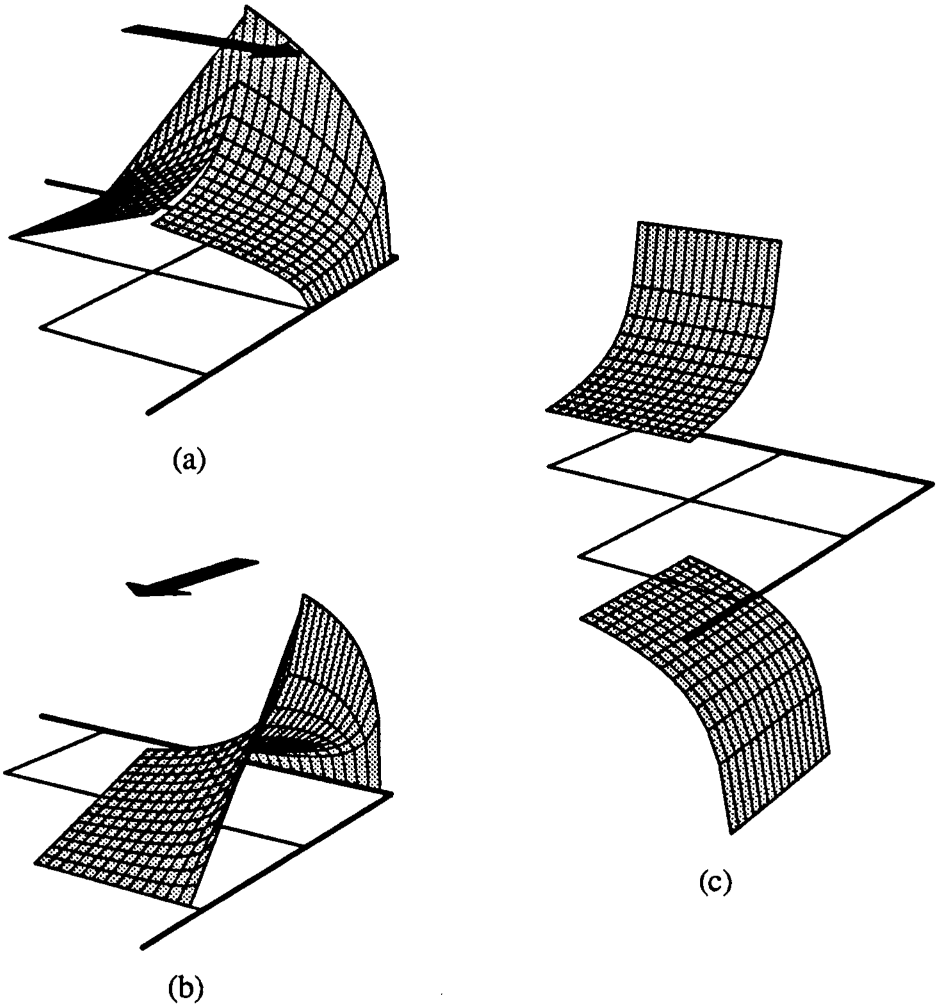
(a)

(b)

(c)

Fig. 8. The corner basis functions used to obtain the correct magnetic singularity. The Cartesian components of the basis function for the tangential current are illustrated by (a) and (b). The corresponding basis function for the charge distribution is shown in (c).

4 Calculation of the matrix elements

The use of complicated basis and testing functions like those described above, makes it is essential to find numerically efficient methods to calculate the matrix elements given by Eq. (16). Each of our basis and testing functions consists of two or three sub-functions. Each matrix element is the sum of the contributions from such sub-functions. The calculation of these "sub-elements" will now be addressed.

Non self-patch terms

As mentioned in the introduction, a multipole method was introduced by the author in Ref. [11] to facilitate the calculation of the matrix elements. Here, an overview of this method is given, see also [11].

The analysis is presented here in three dimensions. The analogous two-dimensional formulation is straightforward. Denote by f and w two functions with compact support

V_f and V_w, respectively. Let the symbol "*" denote multiplication in the case of scalar functions and the scalar product in the case of vector functions, and consider

$$\int_{V_w} \int_{V_f} f(\boldsymbol{r}') * w(\boldsymbol{r})\, G(\boldsymbol{r},\boldsymbol{r}')\, \mathrm{d}v'\, \mathrm{d}v \tag{22}$$

Introduce two spheres circumscribing the volumes V_f and V_w, respectively, and let the centra of these spheres define the origins of two local spherical coordinate systems denoted by K_f and K_w, respectively. Denote space vectors referring to K_f by $\boldsymbol{r}_f$ and those referring to K_w by $\boldsymbol{r}_w$.

Expressed in the coordinates of K_f, the free space Green function can be expanded in the spherical scalar wave functions $\overset{i}{\psi}_{\sigma m l}$ and $\overset{e}{\psi}_{\sigma m l}$ as [17]

$$G(\boldsymbol{r}_f,\boldsymbol{r}_f') = ik \sum_n \overset{i}{\psi}_n(\boldsymbol{r}_f')\, \overset{e}{\psi}_n(\boldsymbol{r}_f) \qquad r_f > r_f' \tag{23}$$

where the summation over n denotes a triple sum over l, m and σ. The definition of the spherical scalar wave functions can be found in Appendix B. Provided the two circumscribing spheres are disjunct the translation properties of the spherical scalar wave functions imply, cf. [11],

$$\int_{V_w} \int_{V_f} f(\boldsymbol{r}') * w(\boldsymbol{r})\, G(\boldsymbol{r},\boldsymbol{r}')\, \mathrm{d}v'\, \mathrm{d}v = ik \sum_{nn'} P_{nn'}(\boldsymbol{R})\, q_n(f) * q_{n'}(w) \tag{24}$$

where $\boldsymbol{R}$ denotes the space vector from the origin of K_f to the origin of K_w. The matrix $P_{nn'}$ is defined in Appendix B. The functional $q_n(f)$ is given by

$$q_n(f) = \int_{V_f} f(\boldsymbol{r})\, \overset{i}{\psi}_n(\boldsymbol{r}_f)\, \mathrm{d}v \tag{25}$$

and $q_n(w)$ is defined analogously. These functionals express the multipole moments associated with the functions f and w.

Eq. (24) can obviously be applied to calculate the bulk of the matrix elements given by Eq. (16) when subdomain basis and testing functions are used. The calculations can be further simplified by expanding the spherical Bessel function $j_l(kr)$ which is a factor in the function $\overset{i}{\psi}_{\sigma m l}$, cf. Appendix B, in a power series as [18]

$$j_l(kr) = \sum_{d=0}^{\infty} c_d \cdot (kr)^{l+2d} \tag{26}$$

Hence $q_n(f)$ can be written

$$q_n(f) = \sum_{d=0}^{\infty} k^{l+2d}\, \overset{d}{q}_n(f) \tag{27}$$

In our case the domain of the integral in Eq. (25) is a flat sub-square. Define a local spherical coordinate system with origin at the centre of sub-square according to Fig. 9.

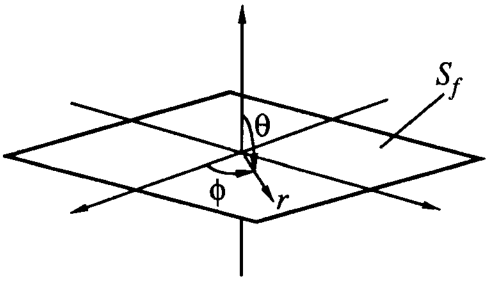

Fig. 9. The local spherical coordinate system used at sub-square when describing the multipole moments.

The volume integrations in the equations above then become surface integrals and we denote the surfaces S_f and S_w, respectively, in analogy with the volume notation above. The multipole moments $\overset{d}{q}_n(f)$ can now be expressed as

$$\overset{d}{q}_{\sigma ml}(f) = \overset{d}{\kappa}_{ml} \int_{S_f} f(r)\, r^{l+2d} \begin{pmatrix}\cos m\phi \\ \sin m\phi\end{pmatrix} \mathrm{d}S \qquad (28)$$

where the coefficients $\overset{d}{\kappa}_{ml}$ are given by

$$\overset{d}{\kappa}_{ml} = \frac{1}{(-2)^d\, d!\,(2l+2d+1)!!}\left(\frac{\varepsilon_m}{2\pi}\,\frac{2l+1}{2}\,\frac{(l-m)!}{(l+m)!}\right)^{1/2} P_l^m(0) \qquad (29)$$

Here P_l^m is the associated Legendre function and $\varepsilon_m=2-\delta_{m0}$, $l=0,1,\dots$, $m=0,\dots l$ and $\sigma=e,o$ (even,odd).

As our sub-squares are small compared to the wavelength it is numerically efficient to calculate $q_n(f)$ using Eq. (27). The functionals $\overset{d}{q}_n(f)$ do not depend on the wavelength, hence they can be calculated and stored for a certain sub-function. Moreover, $\overset{d}{q}_n(f)$ can be calculated analytically for all sub-functions described in Section 3 applying the technique developed to calculate the static term $\overset{0}{q}_n(f)$ in Ref. [11].

The summations in Eq. (24) have to be truncated in the numerical implementation. When n and n' are truncated equally, the reciprocity of the expression (22) is preserved by the multipole method. Hence, the matrix of Eq. (16) will be symmetric when Galerkin's method is used. This leads to increasing efficiency in the numerical treatment.

Special attention has to be paid to the treatment of the matrix sub-elements corresponding to adjacent sub-squares. In general, Eq. (24) does not hold for these elements, since the convergence of the multipole expansion cannot be guarantied. Numerical experiments, cf. [11], show, however, that reasonable accuracy can be obtained.

Self-patch terms

A matrix sub-element containing self-patch terms can be expressed as a power series in the wave number k. Expand the exponential function included in the free space Green function as

$$e^{ik|\boldsymbol{r}-\boldsymbol{r}'|} = \sum_{d=0}^{\infty} \frac{(ik|\boldsymbol{r}-\boldsymbol{r}'|)^{d}}{d!} \tag{30}$$

Now, using the notation above, a sub-element can be expressed

$$\int_{S_w} \int_{S_f} f(\boldsymbol{r}')*w(\boldsymbol{r})\; G(\boldsymbol{r},\boldsymbol{r}')\; \mathrm{d}S'\, \mathrm{d}S = \sum_{d=0}^{\infty} k^{d} \frac{i^{d}}{4\pi\cdot d!} \int_{S_w} w(\boldsymbol{r})* \int_{S_f} f(\boldsymbol{r}')\; |\boldsymbol{r}-\boldsymbol{r}'|^{d-1} \mathrm{d}S'\mathrm{d}S \tag{31}$$

As the sub-squares are small compared to the wavelength, this series converges fast and is numerically efficient. The integrals can be computed and stored for relevant combinations of f and w.

The singularity $1/|\boldsymbol{r}-\boldsymbol{r}'|$ when $d=0$ can be eliminated by evaluating the inner integral using a polar coordinate system centred at the field point $\boldsymbol{r}$.

It should be noticed that for odd values of d the inner integral can be expressed as

$$\int_{S_f} f(\boldsymbol{r}')\; |\boldsymbol{r}-\boldsymbol{r}'|^{d-1} \mathrm{d}S' = \frac{\overset{0}{q}_{e0,d-1}(f;\boldsymbol{r}_f)}{\overset{0}{\kappa}_{0,d-1}} \tag{32}$$

where the notation "$;\boldsymbol{r}_f$" implies that the multipole moments should be evaluated in a coordinate system centred at the field point $\boldsymbol{r}$ and not at the centre of the sub-square which is the case in Eq. (28). These shifted multipole moments can easily be calculated from the non-shifted moments given by Eq. (28) using the translation properties of static multipoles described in Ref. [11].

5 Calculation of the right side

The multipole approach presented above can be used to simplify the calculation of the right side of Eq. (16). It is not difficult to see that when the incident electric field $\boldsymbol{E}^{in}$ is due to a known source distribution at finite distance from the scatterer, the technique described in Section 4 to calculate the matrix elements can be applied to compute the right side elements of Eq. (16). However, in this paper plane wave incidence is considered and a related technique is described below.

Plane wave incidence

Define the incident electric field $\boldsymbol{E}^{in}$ as

$$\boldsymbol{E}^{in}(\boldsymbol{r}) = \boldsymbol{E}_0\, e^{i\boldsymbol{k}\cdot\boldsymbol{r}} \tag{33}$$

This field can be expressed as the field from a point source at infinity.

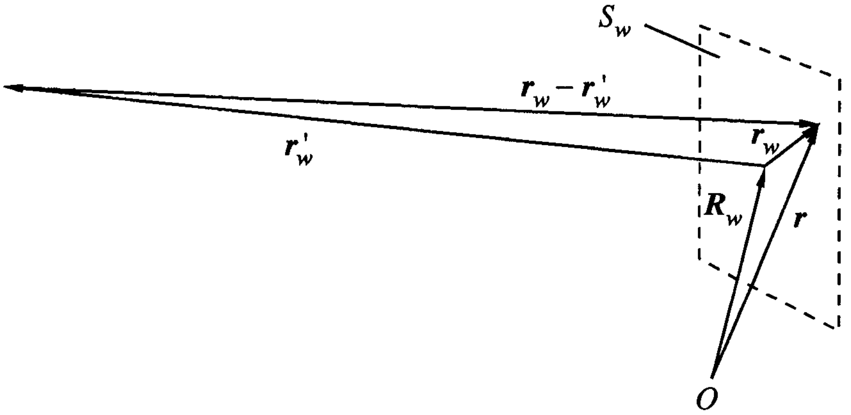

Fig. 10. Definition of the notation of the space vectors.

The vector $\boldsymbol{R}_w$ denotes the position of the centre of a sub-square S_w which contains the support of a testing sub-function $\boldsymbol{w}$, see Fig. 10. The vectors $\boldsymbol{r}_w$ and $\boldsymbol{r}'_w$ denote the field point and the source point, respectively, referring to a local origin at the centre of the sub-square.

Taking the limit as $|\boldsymbol{r}'_w| \to \infty$ the incident electric field can be written

$$\boldsymbol{E}^{in}(\boldsymbol{r}) = \lim_{|\boldsymbol{r}'_w|\to\infty} \boldsymbol{E}_0 \, e^{-ik|\boldsymbol{R}_w+\boldsymbol{r}'_w|} \, |\boldsymbol{r}'_w| \, \frac{e^{ik|\boldsymbol{r}_w-\boldsymbol{r}'_w|}}{|\boldsymbol{r}_w-\boldsymbol{r}'_w|} \tag{34}$$

if we identify $\boldsymbol{k} = -k\hat{\boldsymbol{r}}'_w$. This limit is easily seen from the approximations

$$|\boldsymbol{R}_w + \boldsymbol{r}'_w| \approx |\boldsymbol{r}'_w| + \boldsymbol{R}_w \cdot \hat{\boldsymbol{r}}'_w \tag{35}$$

and

$$|\boldsymbol{r}_w - \boldsymbol{r}'_w| \approx |\boldsymbol{r}'_w| - \boldsymbol{r}_w \cdot \hat{\boldsymbol{r}}'_w \tag{36}$$

The free space Green function can be expanded in the scalar spherical wave functions, cf. Eq. (23), as

$$\frac{e^{ik|\boldsymbol{r}_w-\boldsymbol{r}'_w|}}{|\boldsymbol{r}_w-\boldsymbol{r}'_w|} = 4\pi\, ik \sum_n \psi^i_n(\boldsymbol{r}_w)\, \psi^e_n(\boldsymbol{r}'_w) \tag{37}$$

The asymptotic behaviour of the spherical Hankel function $h_l^{(1)}$, cf. the definition of $\psi^e_{\sigma ml}$ in Appendix B and [18], implies

$$\psi^e_{\sigma ml}(\boldsymbol{r}'_w) = (-i)^{l+1} \frac{e^{ik|\boldsymbol{r}'_w|}}{k|\boldsymbol{r}'_w|}\, Y_n(-\hat{\boldsymbol{k}}) \tag{38}$$

Finally, using that

$$|\boldsymbol{R}_w+\boldsymbol{r}'_w| = |\boldsymbol{r}'_w| - \hat{\boldsymbol{k}}\cdot\boldsymbol{R}_w \tag{39}$$

as $|r_w'| \to \infty$, Eq. (34) can be rewritten

$$E^{in}(r) = E_0\, 4\pi\, e^{ik\cdot R_w} \sum_n (-i)^l \psi_n^i(r_w)\, Y_n(-\hat{k}) \tag{40}$$

Hence, each testing sub-function w will contribute to the right side of Eq. (16) by

$$\int_{S_w} E^{in}(r)\cdot w(r)\,\mathrm{d}S = E_0 \cdot 4\pi\, e^{ik\cdot R_w} \sum_n (-i)^l\, Y_n(-\hat{k})\, q_n(w) \tag{41}$$

where the vector functional q_n is defined by Eq. (25).

6 The scattered field

When the source distributions are found by solving the matrix equation (16), the scattered field can be calculated by Eq. (1). This can be done by simply adding the contributions from the multipoles described in Section 4. At field points very close to the scatterer attention has to be taken not to violate the regions of convergence, i.e., if the field point is inside a circumscribing sphere of one of the sub-squares on the scatterer, the contribution from that sub-square has to be calculated by other means, e.g., numerical integration. However, in this paper only the calculation of the far scattered field is addressed.

The far scattered field

Define a vector function $F(\hat{r})$ by

$$F(\hat{r}) = \int_S J(r')\, e^{-ik\hat{r}\cdot r'}\,\mathrm{d}S' \tag{42}$$

Using the approximation $|r - r'| \approx |r| - \hat{r}\cdot r'$ in the far zone, the magnetic vector potential, cf. Eq. (3), can be written

$$A(r) = \mu \frac{e^{ik|r|}}{4\pi|r|} F(\hat{r}) \tag{43}$$

It can be shown that the far scattered field, given by Eq. (1), can be expressed as

$$E^{sc}(r) = i\omega\mu \frac{e^{ik|r|}}{4\pi|r|} \left(F(\hat{r}) - (F(\hat{r})\cdot\hat{r})\,\hat{r} \right) \tag{44}$$

Denote by $F_f(\hat{r})$ the contribution to $F(\hat{r})$ given by the basis sub-function f with support in the sub-square S_f. Let the space vector R_f denote the position of the centre of the sub-square S_f. $F_f(\hat{r})$ can be expressed using the multipole moments associated with the basis sub-function f. To see this, compare Eq. (42) with the Eqs. (33) and (41). This results in

$$F_f(\hat{r}) = 4\pi\, e^{-ik\hat{r}\cdot R_f} \sum_n (-i)^l\, Y_n(\hat{r})\, q_n(f) \tag{45}$$

where the vector functional $q_n(f)$ is defined by Eq. (25).

7 Numerical results

In this paper we have chosen to study the numerical performance by calculating the radar cross section (RCS). However, the advantages of the basis functions described in Section 3 are likely to be most accentuated when calculating near field quantities. The RCS is, however, important in many practical applications and, hence, efficient methods to compute the RCS is of great interest.

We employ the definition in Ref. [19] for the RCS

$$\sigma(\theta,\phi) = \lim_{r\to\infty} 4\pi r^2 \frac{|E^{sc}|^2}{|E^{in}|^2} \tag{46}$$

where E^{in} is the electric field of an incident plane wave and E^{sc} is the scattered field at the observation point (r,θ,ϕ).

Using Eq. (44) the RCS can be expressed

$$\sigma(\theta,\phi) = \frac{\omega^2 \mu^2}{4\pi} \frac{|F_\theta|^2+|F_\phi|^2}{|E^{in}|^2} \tag{47}$$

The monostatic RCS is calculated using three combinations of basis and testing functions:

LL Linear (rooftop) basis and testing functions all over the plate.

SL Singular basis functions at edges and corners, cf. Section 3, and linear testing functions all over the plate.

SS Singular basis and testing functions at edges and corners.

As the basis functions are the same as the testing functions in the combinations LL and SS these methods agree with Galerkin's method.

The RCS is calculated varying the number of sub-squares from 9 to 256. The results for four different frequencies, normal incidence, are presented in Fig. 11. Two corresponding examples of the RCS, grazing incidence, are showed in Fig. 12. The convergence is, as seen, greatly enhanced when singular basis functions are used.

The basis functions are designed to match the singular properties of the static fields. Hence, the sub-squares have to be small compared to the wave length. This is clearly illustrated by the present results. At low frequencies very few sub-squares are needed to achieve high accuracy, while at higher frequencies the use of few sub-squares give less accurate values.

It can also be noticed that the SS method converges faster than the SL combination at low frequencies, while the opposite seems to be the case at higher frequencies. This is not unexpected as the SS method exaggerate the influence of the sources near the edges and corners which are dominating at low frequencies but are of less importance at higher frequencies.

The current distribution on the plate is plotted in Figs. 13 and 14 using 15×15 sub-squares. The SS distributions are not presented as they are in almost completely agreement with the SL distributions. When the length of the side is 0.5 λ the variation in the direction transverse to the flow of current still has a typical "static" character while at

1 λ the edge behaviour is restricted to a smaller region. It is therefore clear that using just a few sub-squares, the singular basis functions will not approximate the current distribution at higher frequencies well.

Fig. 15 shows the calculated monostatic RCS versus frequency. Also shown are measurements of the RCS presented in Ref. [20]. There is an excellent agreement in the Rayleigh region but a small difference at higher frequencies. The method described in Ref. [6] seems to generally produce slightly lower values than ours, probably due to slower convergence using linear basis functions.

In Figs. 16 and 17 the bistatic RCS is plotted. Two cases of incidence are considered. In Fig. 16 the incidence is normal to the plate while in Fig. 17 the incident angle is 45 degrees. The polarization of the electric field is in both cases parallel to two of the edges of the plate (the polarization is perpendicular to the plane of incidence).

The numerical computations presented in this section clearly show the importance of choosing the appropriate basis functions. The singular basis functions give, in general, more accurate results and also faster convergence. These phenomena are also born out in the computations of the current distribution in Fig. 13, where the use of LL functions leads to anomalies near the edge. The use of singular basis functions does not produce such irregularities.

8 Summary and conclusions

The method of moments is a well-known approach to solve integral equations. The unknown function is expanded in a set of basis functions and a testing procedure is applied. The integral equation is replaced by a truncated matrix equation suited for numerical treatment. When the unknown function has a singular behaviour, the choice of basis functions is of great importance, especially in cases where high accuracy is needed.

In this paper we have treated a canonical problem, the electromagnetic scattering by a thin conducting square plate. We have designed basis functions with correct edge and corner properties. The electric as well as the magnetic singularities have been taking into account. A multipole technique has been applied to simplify the calculation of the matrix elements, the right side of the matrix equation, and the far scattered field. Results have been presented, illustrating the improvement of the numerical convergence when well-suited basis functions are used, and thus reducing the truncation size of the matrix.

The presented combination of singular basis functions and the multipole technique may obviously be applied to a wide range of scattering and transmission problems. The advantages of the method are likely to be still more obvious when near field quantities are studied. Investigations in this area are in progress and will be presented in a forthcoming paper.

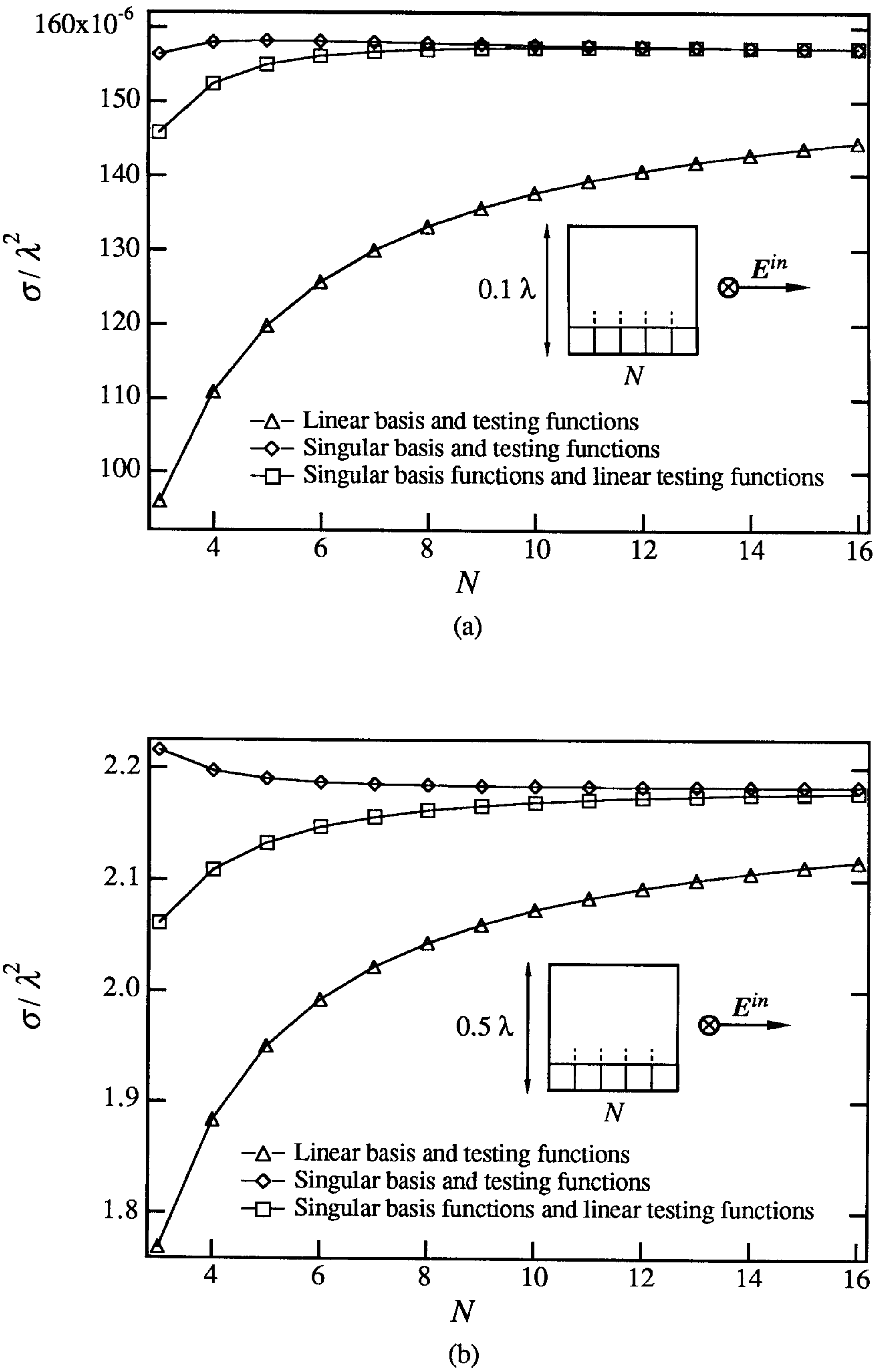

Fig. 11. Calculated values of the monostatic radar cross section, normal incidence, for 4 sizes of the plate: (a) length of side = 0.1 λ, (b) length of side = 0.5 λ and on the following page (c) length of side = 1 λ and (d) length of side = 2 λ. N is the number of sub-squares at each side of the plate, i.e., the total number of sub-squares on the plate is $N \times N$.

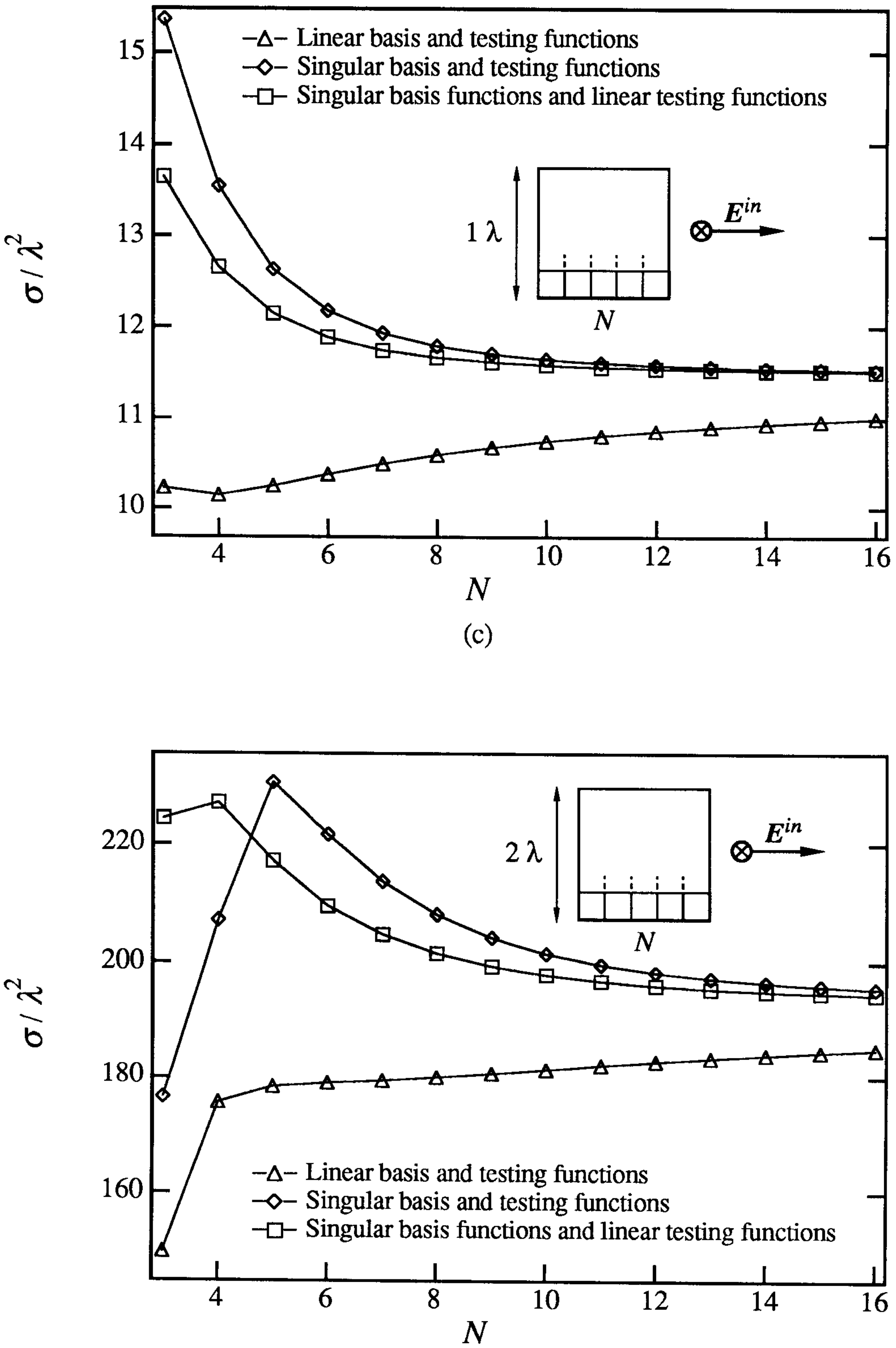

(c)

(d)

Fig. 11 c, d. Captions, see Fig. 11 a,b.

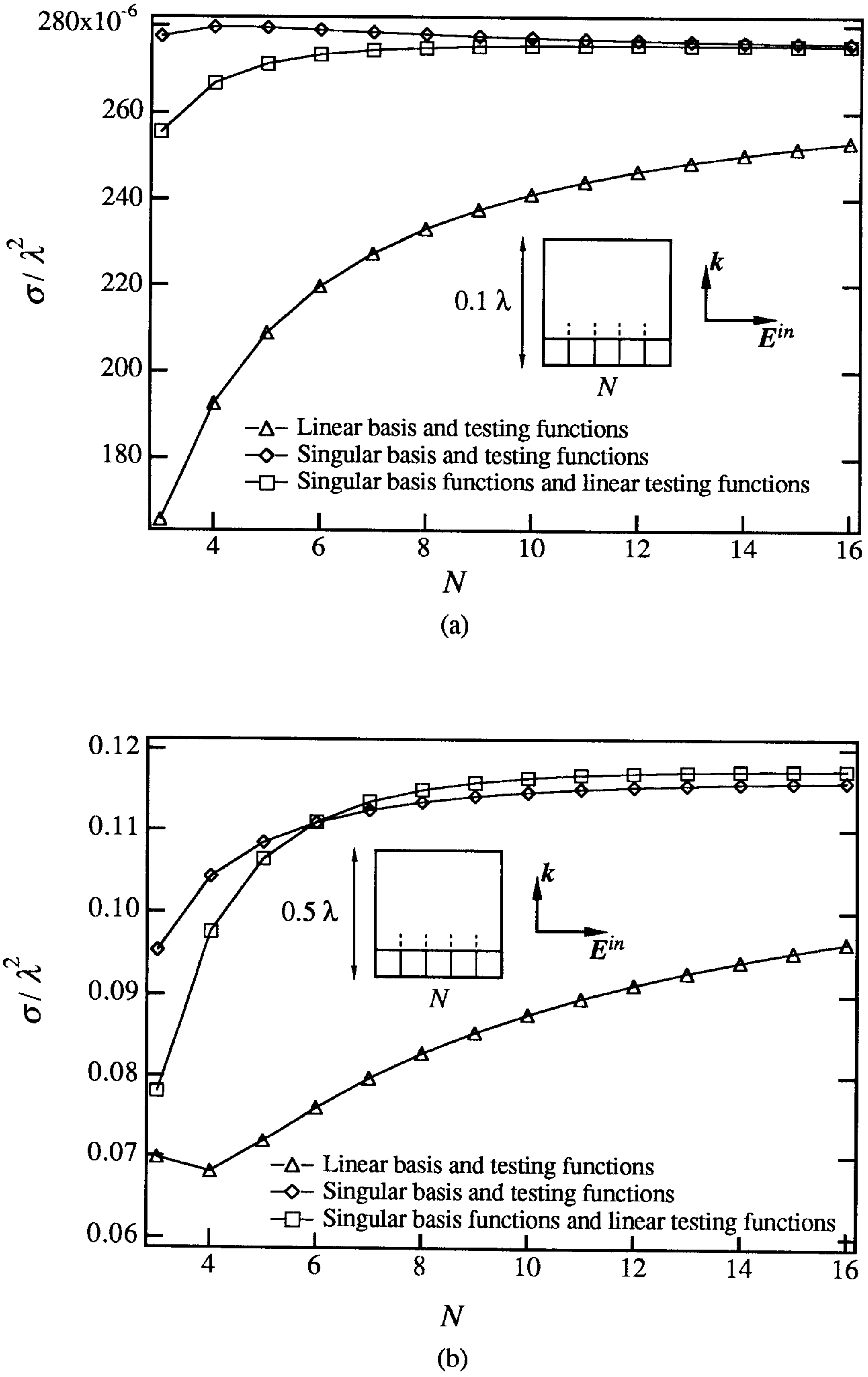

Fig. 12. Calculated values of the monostatic radar cross section, grazing incidence, for 2 sizes of the plate: (a) length of side = 0.1 λ, (b) length of side = 0.5 λ. N is the number of sub-squares at each side of the plate, i.e., the total number of sub-squares on the plate is $N \times N$.

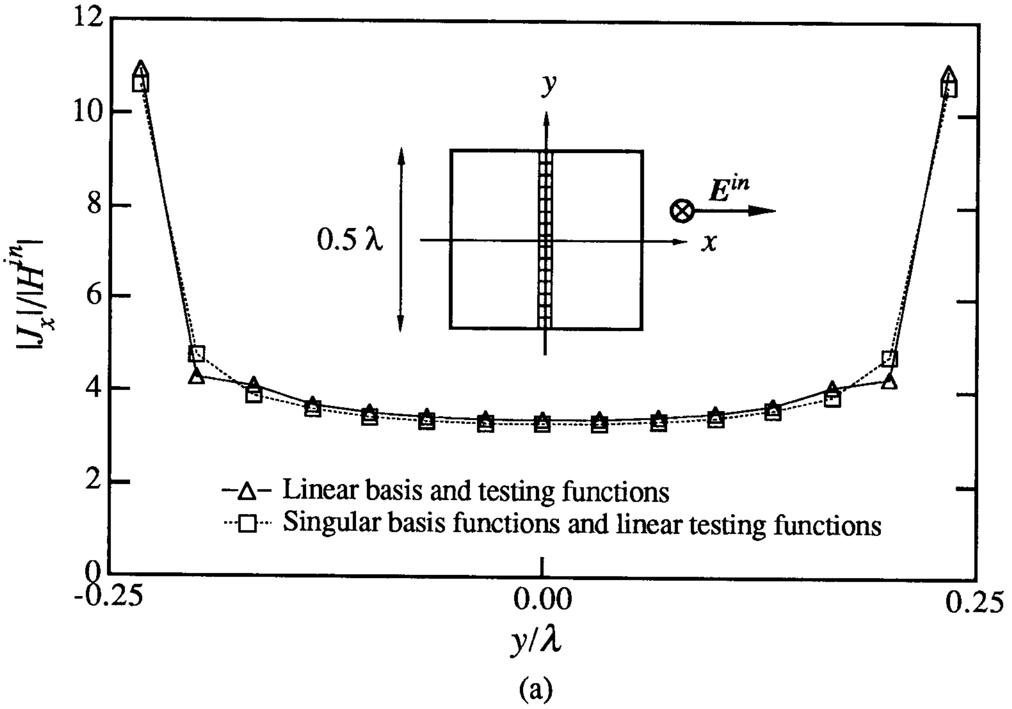

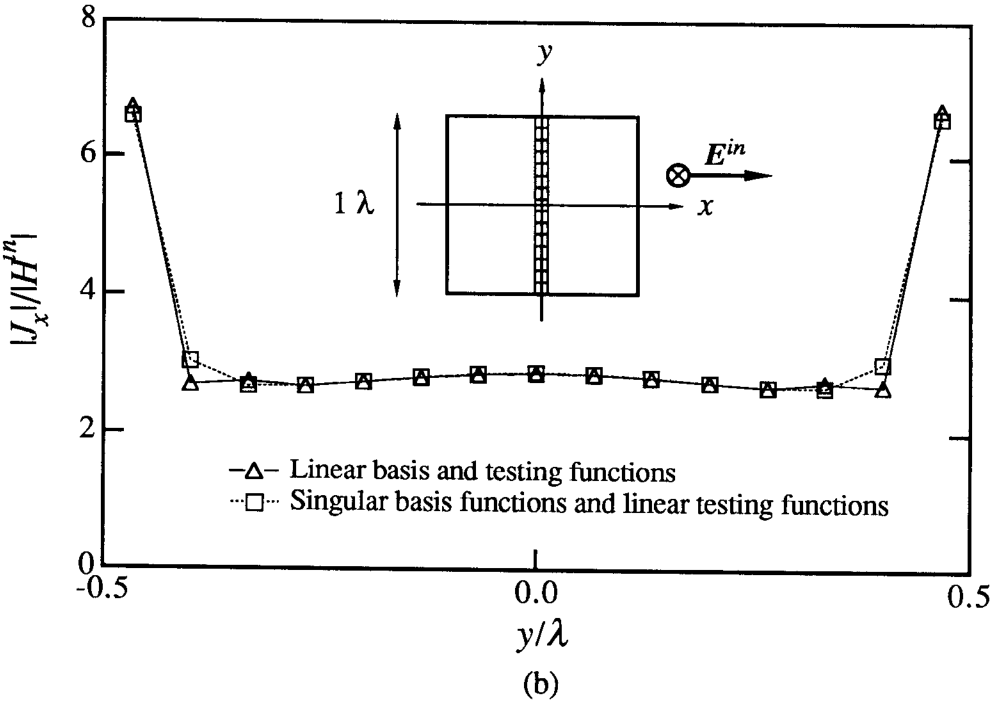

Fig. 13. The current density parallel to the incident electric field, i.e., J_x. The mean values of the current density on the sub-squares in the middle row *transverse* to the direction of the current are shown, i.e., along the y-axis. The length of the side of the plate is (a) 0.5 λ and (b) 1 λ. In both cases the plate is divided into 15 × 15 sub-squares.

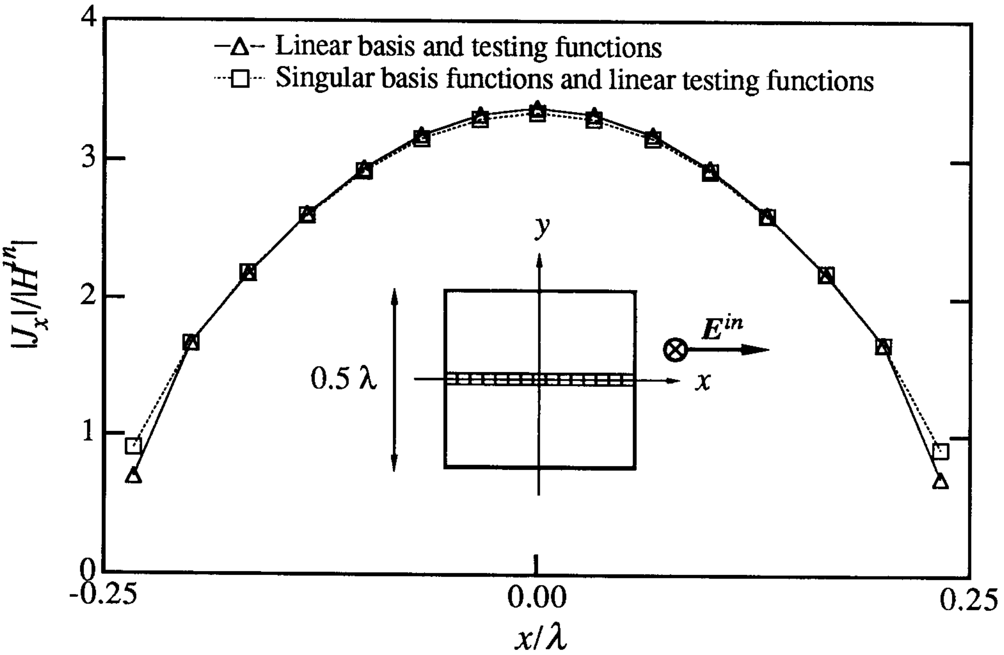

(a)

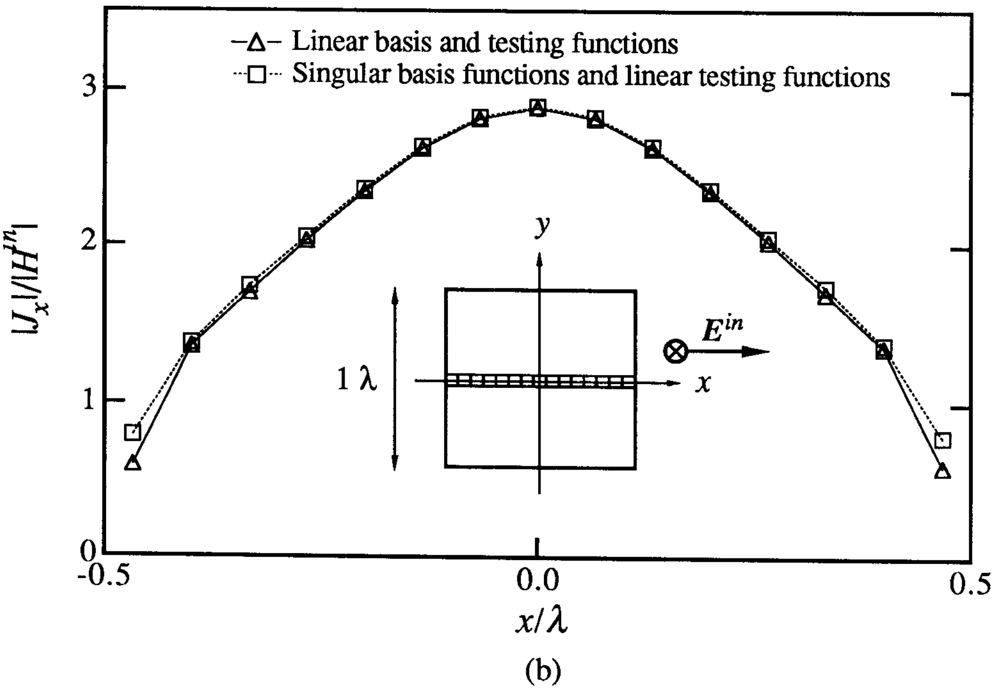

(b)

Fig. 14. The current density parallel to the incident electric field, i.e., J_x. The mean values of the current density on the sub-squares in the middle row *parallel* to the direction of the current are shown, i.e., along the x-axis. The length of the side of the plate is (a) 0.5 λ and (b) 1 λ. In both cases the plate is divided into 15 × 15 sub-squares.

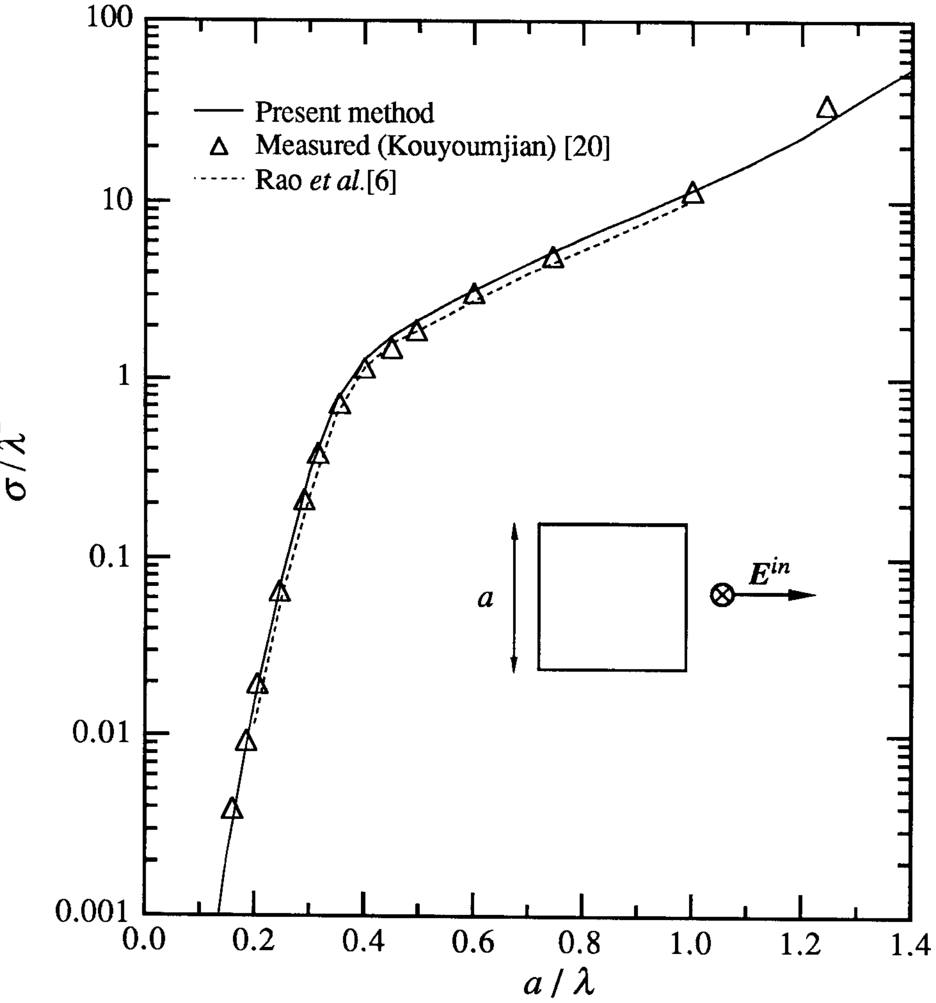

Fig. 15. Monostatic radar cross section versus frequency, normal incidence. Measurements are for plate of thickness 0.000127 λ.

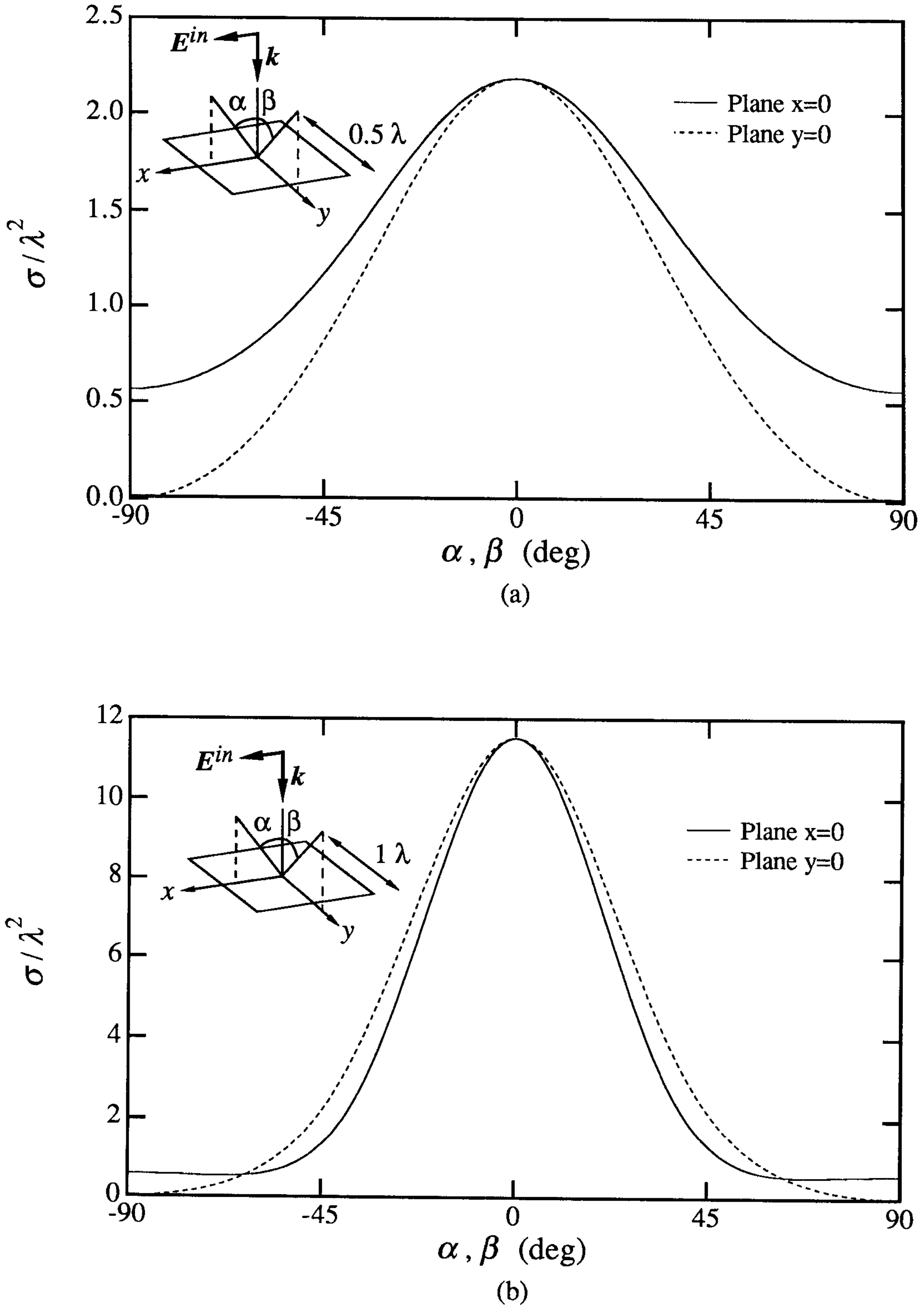

(a)

(b)

Fig. 16. Bistatic radar cross section, normal incidence, for two sizes of the plate: (a) length of side = 0.5 λ and (b) length of side = 1 λ.

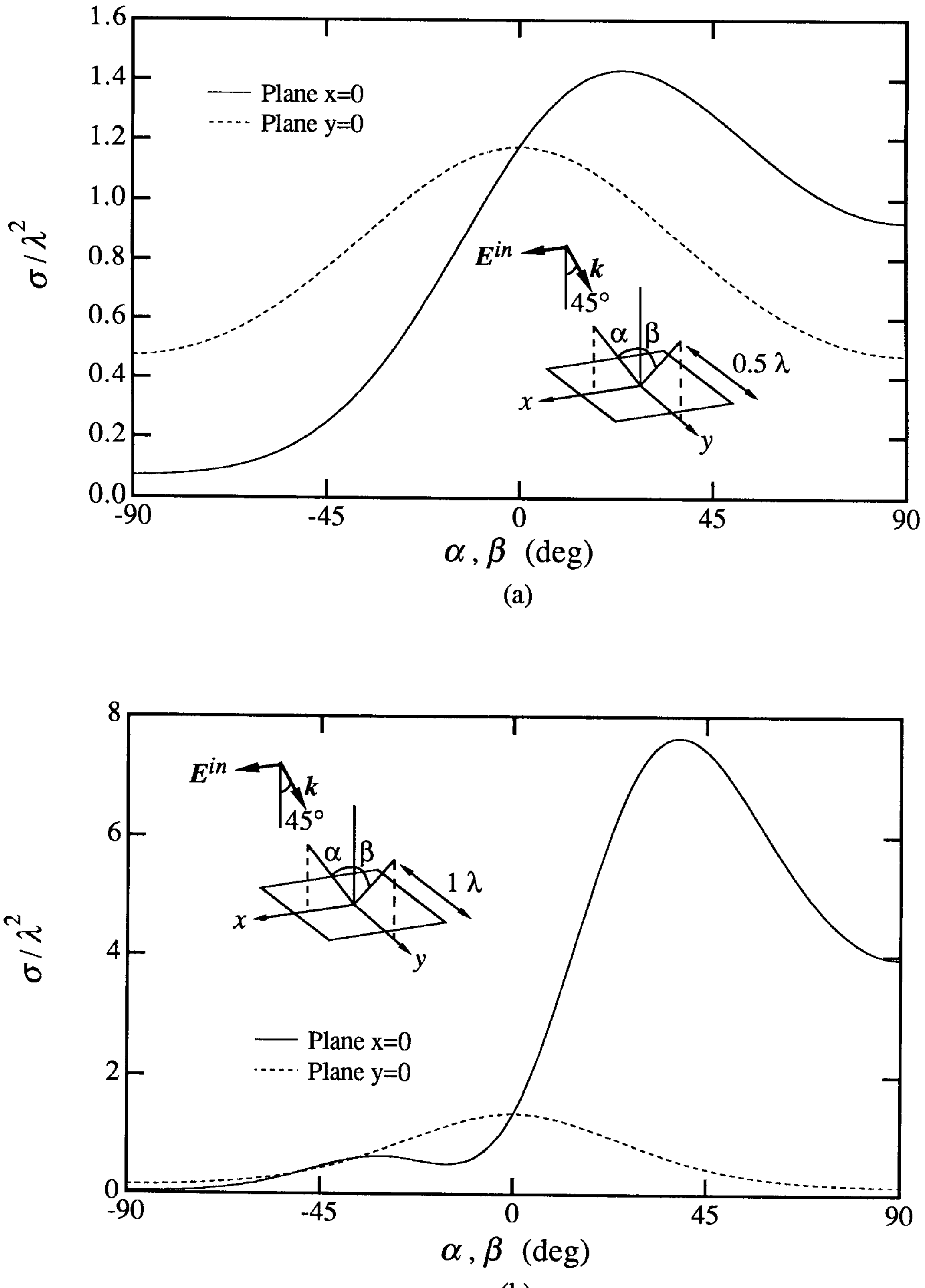

(a)

(b)

Fig.17. Bistatic radar cross section, incident angle = 45 degrees for two sizes of the plate : (a) length of side = 0.5 λ and (b) length of side = 1 λ.

Appendix A

In the caption of Fig. 7, Section 3, it is claimed that the equipotential lines in Fig. 7 enclose equal amount of current due constant difference of potential between the lines. The statement will be shown in this appendix.

Suppose we have a surface current density $\boldsymbol{J}$ on a surface S that can be written

$$\boldsymbol{J} = \hat{\boldsymbol{n}} \times \nabla \Phi \tag{A1}$$

where $\hat{\boldsymbol{n}}$ denotes the unit normal to S and Φ denotes a scalar potential.

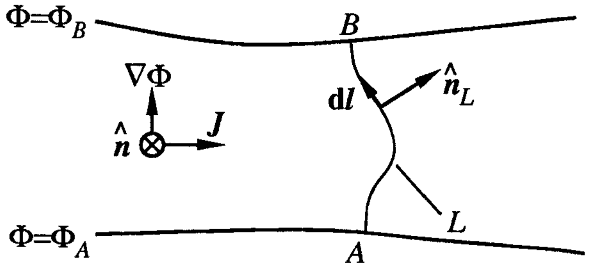

Fig. A1

It is obvious from Eq. (A1) that the equipotential lines $\Phi{=}\Phi_A$ and $\Phi{=}\Phi_B$ represent lines of current, see Fig. A1. The total current I_{AB} enclosed by the curves becomes

$$I_{AB} = \int_L \boldsymbol{J} \cdot \hat{\boldsymbol{n}}_L \, \mathrm{d}l \tag{A2}$$

Using Eq. (A1) and the vector identity

$$(\boldsymbol{a} \times \boldsymbol{b}) \cdot \boldsymbol{c} = (\boldsymbol{c} \times \boldsymbol{a}) \cdot \boldsymbol{b} \tag{A3}$$

the current can be written as

$$I_{AB} = \int_L (\hat{\boldsymbol{n}}_L \times \hat{\boldsymbol{n}}) \cdot \nabla \Phi \, \mathrm{d}l = \int_L \nabla \Phi \cdot \mathbf{d}\boldsymbol{l} = \Phi_B - \Phi_A \tag{A4}$$

Note that the current I_{AB} is independent of the choice of line L between A and B. Every line L will give the same result. As the potential difference is constant between the lines of current in Fig. 7 they enclose the same amount of current.

Appendix B

This appendix contains the definitions of the spherical scalar wave functions and the translation matrix $P_{nn'}$. An exhaustive review of the transformation properties of the scalar wave functions can be found in Ref. [17].

The spherical scalar wave functions

The spherical scalar wave functions are defined as

$$\psi^{i}_{\sigma ml}(\boldsymbol{r}) = j_l(kr)\, Y_{\sigma ml}(\hat{\boldsymbol{r}}) \tag{B1}$$

$$\psi^{e}_{\sigma ml}(\boldsymbol{r}) = h_l^{(1)}(kr)\, Y_{\sigma ml}(\hat{\boldsymbol{r}}) \tag{B2}$$

where j_l is the spherical Bessel function, $h_l^{(1)}$ the spherical Hankel function of the first kind and $Y_{\sigma ml}$ is the spherical harmonic defined by

$$Y_{\sigma ml} = \left(\frac{\varepsilon_m}{2\pi} \frac{2l+1}{2} \frac{(l-m)!}{(l+m)!} \right)^{1/2} P_l^m(\cos\theta) \begin{pmatrix} \cos m\phi \\ \sin m\phi \end{pmatrix} \tag{B3}$$

Here P_l^m is the associated Legendre function and $\varepsilon_m = 2-\delta_{m0}$, $l=0,1,\ldots,$ $m=0,\ldots l$ and $\sigma=e,o$ (even,odd). We employ the definitions in Ref. [18] for the Bessel, Hankel and associated Legendre functions.

The translation matrix $P_{nn'}$

Using spherical coordinates with $\boldsymbol{R} = (R,\eta,\varphi)$ the matrix $P_{nn'}(\boldsymbol{R})$ is given by [17]

$$\begin{aligned} P_{\sigma ml,\sigma m'l'}(\boldsymbol{R}) &= (-1)^{m'} B_{ml,m'l'}(R,\eta) \cos(m-m')\varphi \\ &\quad + (-1)^{\sigma} B_{ml,-m'l'}(R,\eta) \cos(m+m')\varphi \end{aligned} \tag{B4}$$

$$\begin{aligned} P_{\sigma ml,\sigma' m'l'}(\boldsymbol{R}) &= (-1)^{m'+\sigma'} B_{ml,m'l'}(R,\eta) \sin(m-m')\varphi \\ &\quad + B_{ml,-m'l'}(R,\eta) \sin(m+m')\varphi \qquad \sigma \neq \sigma' \end{aligned} \tag{B5}$$

where

$$(-1)^{\sigma} = \begin{cases} 1 & \sigma = e \\ -1 & \sigma = o \end{cases}$$

and

$$\begin{aligned} B_{ml,m'l'}(R,\eta) &= (-1)^{m+m'} \left(\frac{\varepsilon_m \varepsilon_{m'}}{4} \right)^{1/2} \sum_{\lambda=|l-l'|}^{l+l'} (-1)^{(l'-l+\lambda)/2} (2\lambda+1) \\ &\quad \times \left(\frac{(2l+1)(2l'+1)(\lambda-(m-m'))!}{(\lambda+(m-m'))!} \right)^{1/2} \begin{pmatrix} l & l' & \lambda \\ 0 & 0 & 0 \end{pmatrix} \begin{pmatrix} l & l' & \lambda \\ m & -m' & m'-m \end{pmatrix} \\ &\quad \times h_\lambda^{(1)}(kR)\, P_\lambda^{m-m'}(\cos\eta) \end{aligned} \tag{B6}$$

The definition of the Wigner 3-j symbol $\begin{pmatrix} \cdot & \cdot & \cdot \\ \cdot & \cdot & \cdot \end{pmatrix}$ can be found in, e.g., [21].

References

[1] R. F. Harrington, *Field Computation by Moment Methods*, New York: The Macmillan Company, 1968.

[2] J. C. Minor and D. M. Bolle, "Modes in the shielded microstrip on a ferrite substrate transversely magnetized in the plane of the substrate," *IEEE Trans. Microwave Theory Tech.*, vol. 19, no. 7, pp. 570-577, July 1971.

[3] R. Jansen, "A moment method for covered microstrip dispersion," *AEÜ*, Band 29, Heft 1, pp. 17-20, 1975.

[4] T. Andersson, "Calculations of the electrostatic field and potential from a point charge in front of a circular aperture," *Report TEAT-1003*, Dept. of Electromagnetic Theory, Lund Institute of Technology, Sweden, 1989.

[5] R. F. Harrington and J. R. Mautz, "Electromagnetic transmission through an aperture in a conducting plane," *AEÜ*, Band 31, Heft 2, pp. 81-87, 1977.

[6] S. M. Rao, D. R. Wilton and A. W. Glisson, "Electromagnetic scattering by surfaces of arbitrary shape," *IEEE Trans. Antennas Propagat.*, vol. AP-30, no. 3, pp. 409-418, May 1982.

[7] D. R. Wilton and S. Govind, "Incorporation of edge conditions in moment method solutions," *IEEE Trans. Antennas Propagat.*, vol. AP-25, no. 6, pp. 845-850, Nov. 1977.

[8] N. Faché and D. De Zutter, "Rigorous full-wave space-domain solution for dispersive microstrip lines," *IEEE Trans. Microwave Theory Tech.*, vol. 36, no. 4, pp. 731-737, Apr. 1988.

[9] R. De Smedt and J. Van Bladel, "Magnetic polarizability of some small apertures," *IEEE Trans. Antennas Propagat.*, vol. AP-28, no. 5, pp. 703-707, Sept. 1980.

[10] R. De Smedt, "Low frequency scattering through an aperture in a rigid screen - some numerical results," *J. Sound and Vibration*, vol. 75 no. 3, pp. 371-386, 1981.

[11] T. Andersson, "Method of moments and the use of multipole expansion," *J. Electro. Waves Applic.*, vol. 5, no. 11. pp. 1237-1257, 1991.

[12] D. Colton, R. Kress, *Integral equations methods in scattering theory*, New York, John Wiley & Sons, 1983.

[13] J. Meixner, "The behavior of electromagnetic fields at edges," *IEEE Trans. Antennas Propagat.*, vol. AP-20, no. 4, pp. 442-446, July 1972.

[14] E. Vafiadis and J. N. Sahalos, "Fields at the tip of an elliptic cone," *Proc. IEEE*, vol. 72, no. 8, pp. 1089-1091, Aug. 1984.

[15] R. De Smedt and J. Van Bladel, "Field singularities at the tip of a metallic cone of arbitrary cross section," *IEEE Trans. Antennas Propagat.*, vol. AP-34, no. 7, pp. 865-870, July 1986.

[16] J. Van Bladel, *Singular Electromagnetic Fields and Sources*, Oxford, Clarendon Press, 1991.

[17] A. Boström, G. Kristensson and S. Ström, "Transformation properties of plane, spherical, and cylindrical scalar and vector wave functions," in *Field Representations and Introduction to Scattering*; Eds. V. K. Varadan, V. V. Varadan and A. Lakhtakia, vol. 1 , North Holland Publ. (In Press).

[18] M. Abramowitz and I. A. Stegun (Editors), *Handbook of Mathematical Functions*, Applied Mathematics Series No. 55, Washington D.C.: National Bureau of Standards, 1970.

[19] J. J. Bowman, T. B. A. Senior, P. L. E. Uslenghi (Editors), *Electromagnetic and Acoustic Scattering by Simple Shapes*, Amsterdam, North Holland Publ., 1969.

[20] R. G. Kouyoumjian, "The calculation of the echo areas of perfectly conducting objects by the variational method," Ph.D. dissertation, The Ohio State University, 1953.

[21] A. R. Edmonds, *Angular Momentum in Quantum Mechanics*, Princeton N.J.: Princeton Univ. Press, 1957.